Weierstraß-Institut
für Angewandte Analysis und Stochastik

Leibniz-Institut im Forschungsverbund Berlin e. V.

Preprint ISSN 2198-5855

Dynamical regimes in a class A model of a nonlinear mirror mode-locked laser

Andrei G. Vladimirov[1], Anton V. Kovalev[2], Evgeny A. Viktorov[2], Natalia Rebrova[3],

Guillaume Huyet[4]

submitted: February 11, 2019

[1] Weierstrass Institute
Mohrenstr. 39
10117 Berlin
Germany
E-Mail: andrei.vladimirov@wias-berlin.de

[2] ITMO University
14 Birzhevaya line
Saint-Petersburg
199034, Russia
E-Mail: antony.kovalev@gmail.com
evviktor@gmail.com

[3] Department of Physical Sciences
Cork Institute of Technology
Cork, Ireland
E-Mail: nrebrova@gmail.com

[4] Université Côte d'Azur
Centre National de la Recherche Scientifique
Institut de Physique de Nice
06560 Valbonne, France
E-Mail: guillaume.huyet@inphyni.cnrs.fr

No. 2573
Berlin 2019

2010 *Mathematics Subject Classification.* 78A60, 78M35.

2008 *Physics and Astronomy Classification Scheme.* 42.65.Sf, 42.65.Re, 42.60.Fc.

Key words and phrases. Nonlinear mirror mode-locked lasers, delay differential equations, stability analysis, modulational instability, square waves, cavity solitons.

Authors thank D. Turaev for useful discussions. A.V.K. and E.A.V. acknowledge the support by Government of Russian Federation (Grant 08-08). A.G.V. acknowledges the support of the Fédération Doeblin CNRS, SFB 787 of the DFG, project B5, and Grant No. 14-41-00044 of the Russian Science Foundation.

Edited by
Weierstraß-Institut für Angewandte Analysis und Stochastik (WIAS)
Leibniz-Institut im Forschungsverbund Berlin e. V.
Mohrenstraße 39
10117 Berlin
Germany

Fax: +49 30 20372-303
E-Mail: preprint@wias-berlin.de
World Wide Web: http://www.wias-berlin.de/

Dynamical regimes in a class A model of a nonlinear mirror mode-locked laser

Andrei G. Vladimirov, Anton V. Kovalev, Evgeny A. Viktorov, Natalia Rebrova, Guillaume Huyet

Abstract

Using a simple delay differential equation model we study theoretically the dynamics of a unidirectional class-A ring laser with a nonlinear amplifying loop mirror. We perform analytical linear stability analysis of the CW regimes in the large delay limit and demonstrate that these regimes can be destabilized via modulational and Turing-type instabilities, as well as by a bifurcation leading to the appearance of square-waves. We investigate the formation of square-waves and mode-locked pulses in the system. We show that mode-locked pulses are very asymmetric with exponential decay of the trailing and superexponential growth of the leading edge. We discuss asymmetric interaction of these pulses leading to a formation of harmonic mode-locked regimes.

1 Introduction

The possibility of generation of short light pulses by locking the longitudinal modes of a laser was discussed only a few years after the laser discovery. Mode-locking techniques can be classified into two categories: (i) active mode locking, where synchronization of the modes is achieved by introducing an external modulation at a frequency close to the cavity free spectral range and (ii) passive mode locking where a nonlinear component reduces losses for pulsed operation with respect to continuous-wave (CW) regimes. Compact two-section semiconductor lasers are examples of passively mode-locked lasers. Unlike actively mode-locked and hybrid mode-locked lasers, they do not requeire an external radio frequency source for their operation. A standard method to study theoretically the properties of mode-locked semiconductor devices is based on direct integration of the so-called traveling wave equations describing space-time evolution of the electric field and carrier density in the laser sections [3–5, 19]. Another, much simpler approach for theoretical analysis of mode-locking based on the derivation of amplitude equations was developed by Haus and co-workers [6]. The drawback of the Haus master equations is, however, that they rely on certain simplifying assumptions that are hardly ever realistic for semiconductor devices. To overcome this limitation the third approach was developed in [25–27] based on the use of the so-called lumped element method that allows to derive a delay differential equations for the temporal evolution of the electric field envelope at some fixed position along the cavity axis coupled to the equations for cumulative gain and loss in the amplifying and absorbing laser sections. This approach was found to successfully describe the dynamics of multi-section mode-locked semiconductor lasers [2, 11, 15, 20, 21, 23], frequency swept light sources [13, 17, 18], optically injected lasers [14, 16], semiconductor lasers with feedback [7, 8, 12], as well as some other multimode laser devices [22].

Here by considering an example of a simple model of nonlinear mirror mode-locked laser, we show that the applicability domain of the DDE models is not restricted to passive mode-locking by a saturable absorber, but can be extended to describe other mode-locking mechanisms as well. We study a DDE

DOI 10.20347/WIAS.PREPRINT.2573 Berlin 2019

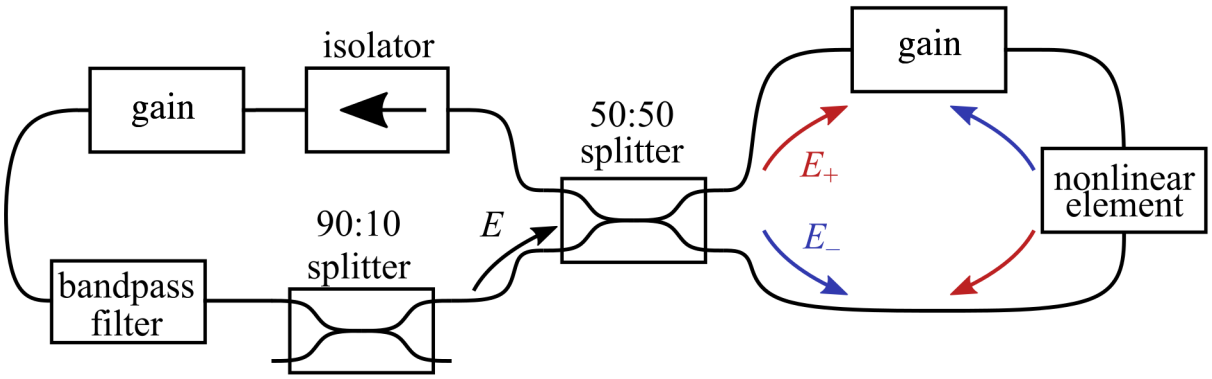

Figure 1: The scheme of a ring laser with gain media, bandpass filter, and non-linear element in a Sagnac interferometer forming a non-linear mirror. Labeled arrows show different propagation directions inside the interferometer.

model of a class-A laser with nonlinear mirror loop in the figure of eught configuration. We show that this model can exhibit different dynamical regimes including square wave formation and generation of short optical pulses, which are always bistable with the non-lasing state. Such pulses could also be considered as temporal cavity solitons or nonlinear temporally localized structures of light [10, 11]. We perform linear stability analysis of CW solutions of the DDE laser model and and reveal modulational and Turing-type instabilities, as well as a bifurcation responsible for the emergence of square waves. Experimental evidence of square wave formation in a mode-locked laser with nonlinear loop mirror was reported in [1]. To study the square waves in the system we construct one-dimensional map exhibiting a period doubling route to chaos. We show that the mode-locked pulses are asymmetric with a super-exponential growth at the leading edge and an exponential decay rate of the trailing edge. We discuss the repulsive interaction of such asymmetric pulses leading to the formation of a harmonic mode-locked regimes.

2 Model equation and CW solutions

A schematic of a mode-locked ring laser cavity that includes a gain medium, a spectral filter, and a non-linear mirror loop in the figure of eught configuration, is given in Fig. 1. This scheme corresponds to experimentally implemented setups of mode-locked lasers with a high-Q microring resonator [9] and an integrated waveguide [1] acting as nonlinear elements. To describe the essential features the device shown in Fig. 1 we consider a very simple DDE model which assumes that the carrier density in the gain media can be adiabatically eliminated. This model governing the time evolution of the complex electric field envelope $E(t)$ reads:

$$\gamma^{-1}\frac{dE}{dt} + E = \frac{\sqrt{\kappa}}{2} e^{g_0/[2(1+|E(t-T)|^2)]} f(|E(t-T)|^2) E(t-T). \tag{1}$$

Here γ is the spectral filter bandwidth, κ is the linear attenuation factor describing nonresonant cavity losses, g_0 is the pump parameter, and the delay parameter T is equal to the cold cavity round trip time. The function f describing the nonlinear mirror reflectivity is defined by

$$f(|E(t-T)|^2) = 1 - e^{ia|E(t-T)|^2},$$

where a is the parameter characterizing the phase shift introduced by the nonlinear mirror loop. In the following we will show that despite being very simple, our model equation (1) is capable of reproducing such experimentally observed behaviours as mode-locking and square wave generation [1].

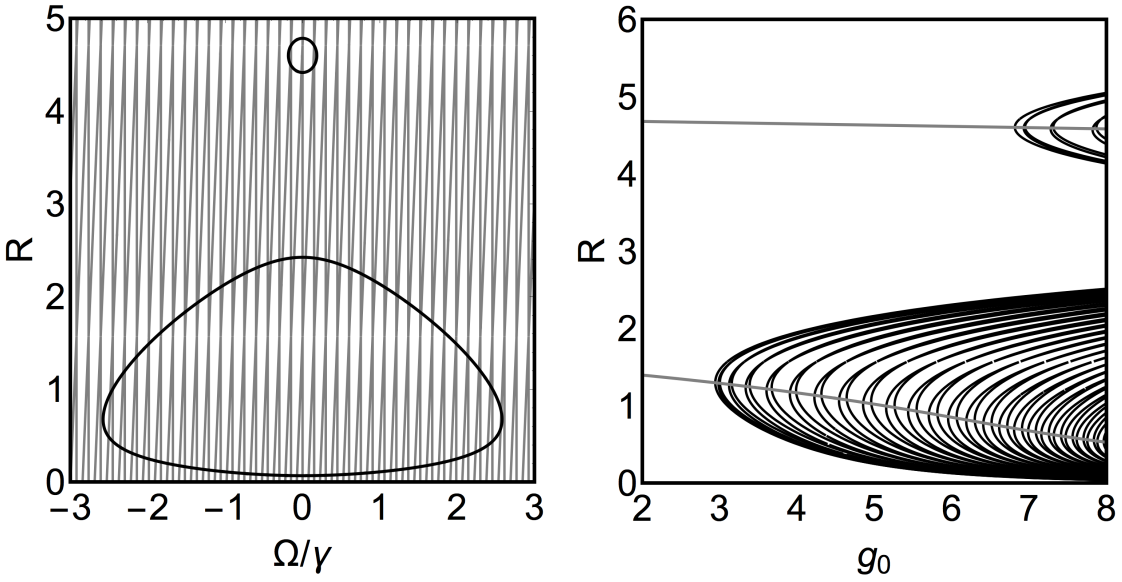

Figure 2: Left: CW solutions at fixed pump parameter $g_0 = 5.0$. CW solutions lie on the intersections of the closed black curves [solutions of Eq. (2)] with thin gray lines [solutions of Eq. (3)]. Other parameter values: $a = 2$, $\gamma = 1$, $\kappa = 0.3$, and $T = 20$. Right: Branches of CW solutions corresponding to different longitudinal laser modes (black lines). Two gray lines are defined by the condition (4). They intersect CW branches at the saddle-node bifurcation points. Lower parts of the CW branches lying below the saddle-node bifurcation points are always unstable, while upper parts can be either stable or unstable.

The simplest solution of Eq. (1) is that corresponding to laser off state, $E = 0$. Linear stability analysis of this trivial non-lasing solution indicates that it is always stable, which means that the laser is non-self-starting for all possible parameter values. Non-trivial CW solutions are defined by the relation $E = \sqrt{R}e^{i\Omega t}$, where $R = |E|^2 > 0$ is the intensity and Ω is the frequency detuning of CW regime from the reference frequency coinciding with the central frequency of the spectral filter. R and Ω satisfy two transcendental equations

$$\kappa e^{\frac{g_0}{1+R}} \sin^2\left(\frac{aR}{2}\right) = 1 + \frac{\Omega^2}{\gamma^2}, \tag{2}$$

$$\tan\left(\frac{aR^2}{2} + T\Omega\right) + \frac{\gamma}{\Omega} = 0, \tag{3}$$

Multiple solutions of these equations are illustrated in the left panel of Fig 2, where CW regimes correspond to the intersections of black closed curves obtained by solving Eq. (2) and thin gray lines obtained from Eq. (3). Right panel of Fig. 2 shows the branches of non-trivial CW solutions as functions of the pump parameter g_0. The lower parts of these branches below the saddle-node bifurcation points defined by the condition

$$g_0 = \tilde{g} \equiv a(1+R)^2 \cot\left(\frac{aR}{2}\right) \tag{4}$$

together with (2) and (3) are always unstable.

3 CW stability in the large delay limit

To study the stability of the upper parts of the CW branches shown in the right panel of Fig. 2 we use the large delay limit approach described in Ref. [28]. By linearizing Eq. (1) on a CW solution given by $E = \sqrt{R}e^{i\Omega t}$ we obtain the characteristic equation in the form:

$$c_2 Y^2 + 2c_1(\lambda)Y + c_0(\lambda) = 0, \tag{5}$$

where $Y = e^{-\lambda T}$ and $c_{0,1,2}$ are given in the Appendix. In the large delay limit, $\gamma T \gg 1$, the eigenvalues belonging to the so-called *pseudo-continuous spectrum* can be represented in the form:

$$\lambda = i\lambda_0 + \frac{\lambda_1}{T} + \mathcal{O}\left(\frac{1}{T^2}\right), \quad \lambda_1 = \lambda_{11} + i\lambda_{12},$$

with real λ_0, λ_{11}, and λ_{12}. Therefore, using the approximate relations $c_{0,1,2}(\lambda) \approx c_{0,1,2}(i\lambda_0)$ and $Y \approx e^{-i\lambda_0 T - \lambda_1}$ we can solve the characteristic equation to express λ_{11} as a function of λ_0 [28]

$$\lambda_{11}^{\pm} = \mathrm{Re}\,\lambda_1^{\pm} = \mathrm{Re}\ln\left(Y_{\pm}^{-1}\right), \quad Y_{\pm} = \frac{-c_1(i\lambda_0) \pm \sqrt{c_1(i\lambda_0)^2 - c_0(i\lambda_0)c_2}}{c_2}. \tag{6}$$

Two solutions $\lambda_{11}^{\pm}(\lambda_0)$ given by Eq. (6) define two branches of pseudo-continuous spectrum shown in the left panel of Fig. 3. Due to the phase shift symmetry of the model equation (1) $E \to Ee^{i\phi}$ with arbitrary constant ϕ one of these branches is tangent to the $\lambda_{11} = 0$ axis on the (λ_0,λ_{11})-plane at the point $\lambda_0 = 0$, i.e., $Y_-^{-1}|_{\lambda_0=0} = 1$. The right panel of Fig. 3 shows the stability diagram of the upper branches of CW solutions on the plane of two parameters: CW solution frequency offset Ω and pump rate g_0. CW solutions are stable (unstable) in the dark (light) gray domains. Black line indicates the saddle-node bifurcation, where two CW solutions merge and disappear. Below this line there are no CW solutions while above it a pair of CW solutions is born with one them corresponding to smaller intensity R being always unstable. Similarly to the case of Eckhaus instability the upper branch of CW solutions can be stable only within the so-called Busse balloon (region labelled "1ïn Fig. 3) limited from below by modulational instability curve shown by blue line. The modulational instability curve is defined by the condition that one of the two branches of the pseudo-continuous spectrum, which satisfies the relation $\left(\lambda_{11}^-\right)_{\lambda_0=0} = \left(d\lambda_{11}^-/d\lambda_0\right)_{\lambda_0=0} = 0$, changes the sign of its curvature at the point $\lambda_0 = 0$, i.e., $\left(d^2\lambda_{11}^-/d\lambda_0^2\right)_{\lambda_0=0} = 0$. The latter condition can be rewritten in the form:

$$\frac{\left[a(1+R)^2\Omega + \gamma(\tilde{g} - g_0)\right]^2}{\left(\gamma^2 + \Omega^2\right)^2} + \frac{(1+R)^2\Omega^2 \csc^2\left(\frac{aR}{2}\right)\left[g_0^2 + 2a^2(1+R)^4 - g_0^2\cos(aR) - 2ag_0(1+R)^2\sin(aR)\right]}{R(\tilde{g} - g_0)\left(\gamma^2 + \Omega^2\right)^2} = 0. \tag{7}$$

where $\tilde{g}$ is defined by (4). It is seen from the figure that the modulation instability curve is tangent to the saddle-node bifurcation line at $\Omega = 0$ and that this curve becomes asymmetric sufficiently far away from the tangency point.

The upper boundary of the CW stability domain shown in the right panel of Fig. 3 consists of two parts separated by codimension-two point C_+. The right part this boundary lying between the points C^+ and C is indicated by red line and corresponds to the so-called Turing-type (wave) instability, where one of the two branches of pseudo-continuous spectrum touches the $\lambda_{11} = 0$ axis at two symmetric points with $\lambda_0 \neq 0$, i.e., $\lambda_{11}^+ = 0$, at $\lambda_0 = \pm\lambda_0^*$ with $\lambda_0^* > 0$. The left part of the stability boundary

lying between two symmetric codimension-two points $C^{\pm}$ is shown by green line and corresponds to a bifurcation of square waves from CW regimes. It is defined by the condition

$$Y_{+}^{-1}|_{\lambda_0=0} = -1, \tag{8}$$

which can be rewritten in the form:

$$2 - \frac{g_0 R}{(1+R)^2} + aR\cot\left(\frac{aR}{2}\right) = 0. \tag{9}$$

The codimension-two points $C_{\pm}$ are defined by Eq. (9) together with additional conditions $\left(d^2\lambda_{11}^{\pm}/d\lambda_0^2\right)_{\lambda_0=0} = 0$. Using the relation (9) the additional conditions can be rewritten as

$$\Omega^2 \pm \gamma\Omega aR = \gamma^2. \tag{10}$$

An implicit equation for the coordinates of $C_{\pm}$ on the (Ω,g_0)-plane are obtained by solving Eq. (10) for R and substituting the resulting solution into Eq. (9). It follows from Eq. (10) that the codimension-two points $C^{\pm}$ shown in the right panel of Fig (3) are symmetric with respect to $\Omega = 0$ axis. The two parts of the square-wave bifurcation curve lying to the left of the point C^{-} and to the right of the point C^{+} correspond to bifurcations from unstable CW solutions. Hence, they give birth to unstable square waves.

Let us consider the CW solution corresponding to the central longitudinal mode with zero detuning from the central frequency of the spectral filter, $\Omega = 0$. For this solution the two quantities $Y_{\pm}$ in Eq. (6) take the form

$$Y_{-}|_{\Omega=0} = 1 - i\frac{\lambda_0}{\gamma}, \tag{11}$$

$$Y_{+}|_{\Omega=0} = \frac{1 - i\lambda_0/\gamma}{1 + aR\cot\left(\frac{aR}{2}\right) - \frac{g_0 R}{(1+R)^2}}. \tag{12}$$

From Eq. (11) we get the relations $Y_{-}|_{\Omega=0,\lambda_0=0} = 1$ and $Y_{-}|_{\Omega=0,\lambda_0\neq 0} < 1$ meaning that the first branch of the pseudo-continuous spectrum of the central longitudinal mode is always stable and is tangent to the imaginary axis at $\lambda_0 = 0$. On the other hand, from Eq. (12) we see that the saddle-node bifurcation of the central longitudinal mode defined by the condition $Y_{+}^{-1}|_{\Omega=0,\lambda_0=0} = 1$ coincides with Eq. (4). Similarly the bifurcation responsible for the emergence of square-waves is defined by the condition $Y_{+}^{-1}|_{\Omega=0,\lambda_0=0} = -1$ coinciding with Eq. (9). As it will be shown in the next section, the condition (9) defines also the period doubling bifurcation of a 1D map, which we construct in the next section to study the the square wave formation in the DDE model Eq. (1).

4 1D map and square waves

The existence of stable square wave solutions in Eq. (1) can be demonstrated by constructing a 1D map that exhibits a period doubling bifurcation corresponding to the emergence of square wave in the DDE model (1). To this end we rescale the time $\tau = t/T$ in Eq. (1) and obtain

$$\varepsilon\frac{dE}{d\tau} + E = \frac{\sqrt{\kappa}}{2} e^{g_0/[2(1+|E(\tau-1)|^2)]} f(|E(\tau-1)|^2) E(\tau-1), \tag{13}$$

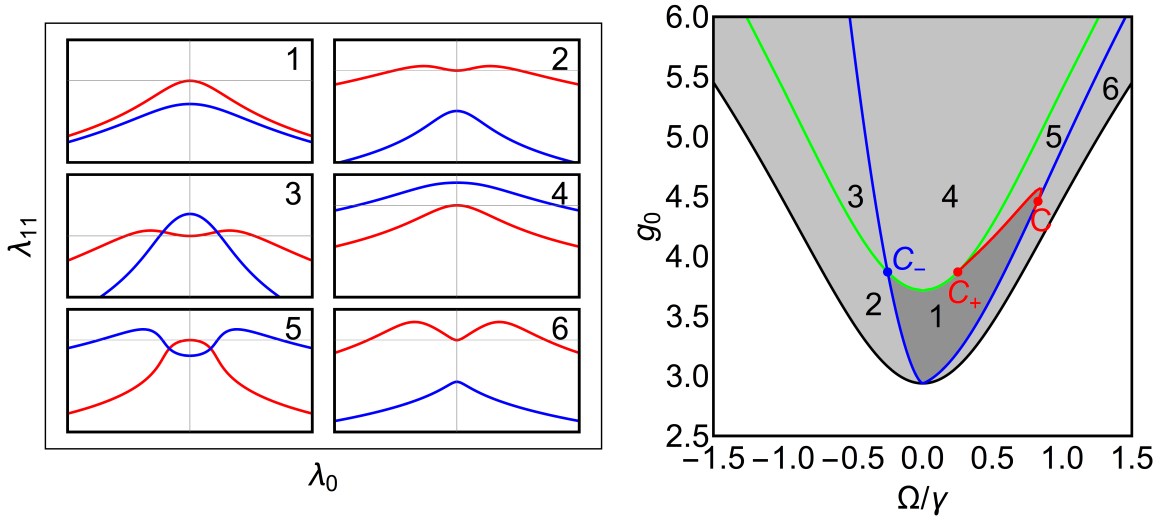

Figure 3: Left: Two branches of pseudo-continuous spectrum. Different numbers illustrate qualitative behaviour of the branches in numbered parameter domains of the right panel. Right: Bifurcation diagram on the plane of two parameters: CW frequency offset Ω and pump parameter g_0, obtained in the limit of large delay time. Black – saddle-node bifurcation curve defined by Eq. (4), blue – modulational instability curve, which serves as a boundary of the Busse balloon and is defined by Eq. (7), green – "square wave" instability defined by Eq. (8), red – Turing-type (wave) instability. $C_\pm$ are codimension-two points defined by Eqs. (9) and (10). CW solutions are stable (unstable) in dark gray region labeled "1"(light gray regions).

where in the large delay limit we have $\varepsilon \equiv 1/\gamma T \ll 1$. By discarding the time derivative term, which is proportional to the small parameter ε, we transform this equation into a map describing the transformation of the electric field envelope E after a round trip in the cavity:

$$R_{n+1} = h(R_n), \quad h(R_n) = \kappa e^{\frac{g_0}{1+R_n}} \sin^2\left(\frac{aR_n}{2}\right) R_n, \tag{14}$$

where $R_n \equiv |E(n)|^2$ with fixed points $R_n = R$ satisfying the condition $R = h(R)$:

$$\kappa e^{\frac{g_0}{1+R}} \sin^2\left(\frac{aR}{2}\right) = 1, \tag{15}$$

which is equivalent to Eq. (2) taken at $\Omega = 0$. Since $\Omega = 0$ is a solution of Eq. (3), fixed points of the map (14) have the same intensities R as those of the central longitudinal mode, i.e. the CW solution of Eq. (1) with zero frequency offset $\Omega = 0$ from the central frequency of the spectral filter. Furthermore, for sufficiently large g_0 a stable fixed point of the map (14) exhibits a period doubling bifurcation which is defined by

$$1 - \frac{g_0 R}{(1+R)^2} + aR \cot\left(\frac{aR}{2}\right) = -1, \tag{16}$$

together with (15). Note, that the relations (15) and (9) are equivalent to (2) and (8) evaluated at $\Omega = 0$. Hence, the period doubling bifurcation point of the map (14) coincides in the limit of large delay with the square wave bifurcation of the longitudinal mode having zero frequency offset, $\Omega = 0$. Since the square waves bifurcation curve in the right panel of Fig. 3 is symmetric with respect to $\Omega \to -\Omega$ the central mode is the first mode undergoing a square wave bifurcation with the increase of the

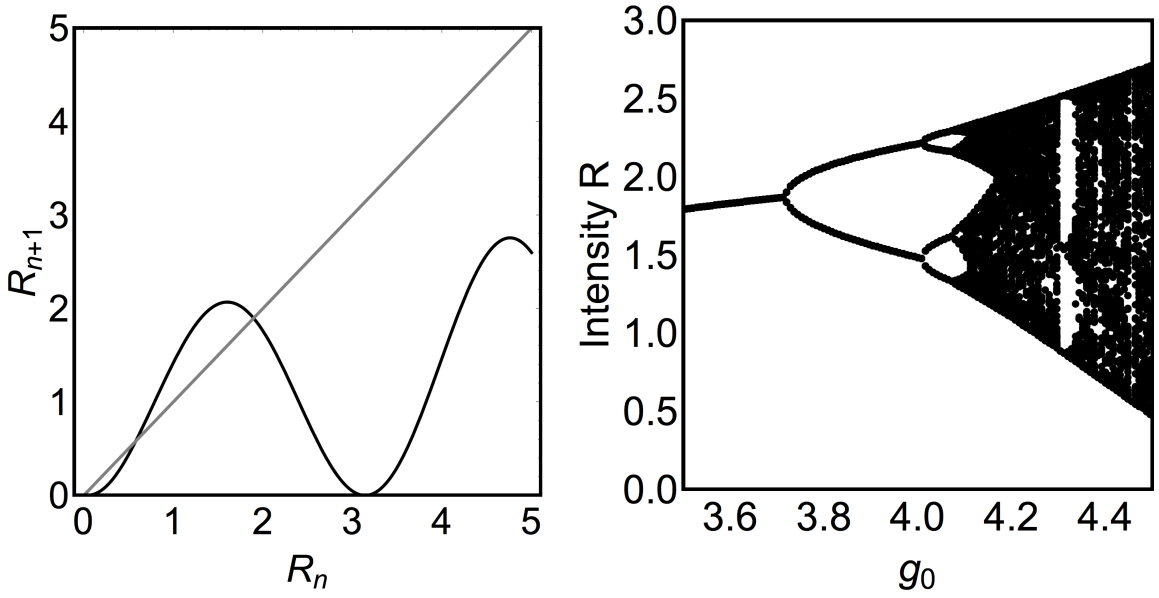

Figure 4: Left: Graph of the function h defined by Eq. (14). Two period one fixed points of the map correspond to the intersections of the black curve with straight gray line $R_{n+1} = R_n$. These fixed point correspond to the of Eq. (1) lying on the upper and lower part of the CW branch with zero frequency offset $\Omega = 0$. Right: Bifurcation diagram illustrating period-doubling route to chaos in the map (14).

pump parameter g_0. The larger is the frequency offset of the mode, the higher is the square wave bifurcation threshold for this mode. When, however, positive (negative) frequency offset is sufficiently large the modes are already unstable with respect to Turing (modulational) instability at the square wave instability point. In this case the square wave bifurcation results in the appearance of unstable square waves. Graphical representation of function h defined by (14) is shown in left panel of Fig. 4, while the right panel of this figure illustrates the period doubling transition to chaos in the 1D map (14).

Period-doubling route to chaos obtained by numerical integration of the DDE model (1) is illustrated in left panel of Fig. 5, where local maxima of the electric field intensity time-trace $R = |E(t)|^2$ are plotted versus increasing values of the pump parameter g_0. It is seen that the diagram in this figure is very similar to that obtained with the 1D map (14), cf. Fig. 4. Note, however, that the period doubling threshold is slightly higher in Fig. 5 than in Fig. 4. This can be explained by taking into consideration that in the DDE model (1) the threshold of the bifurcation leading to the emergence of square waves increases with the absolute value of the frequency detuning Ω. Therefore, we can conclude that in Fig. 5 the CW solution undergoing the period-doubling cascade must have a small non-zero frequency detuning, $\Omega \neq 0$. The first period doubling bifurcation in the left panel of Fig. 4 is responsible for the formation of square waves shown in the right panel of Fig. 4, while further period doublings give rise to more complicated square wave patterns with larger periods. Finally, we note that with the increase of the gain parameter g_0 new pairs of fixed points of the map (14) appear in saddle-node bifurcations. For example, the second pair of fixed points corresponds to the second (right) maximum of the function h shown in the left panel of Fig. 4 and to additional branches of CW solutions visible in the upper right part of the right panel of Fig. 2. Although the linear stability analysis performed in the previous section is applicable to bifurcation analysis of these additional high intensity CW branches as well, in this paper we restrict our consideration to the stability properties of low intensity CW solutions corresponding to moderate values of the pump parameter $g_0 \lesssim 6.5$.

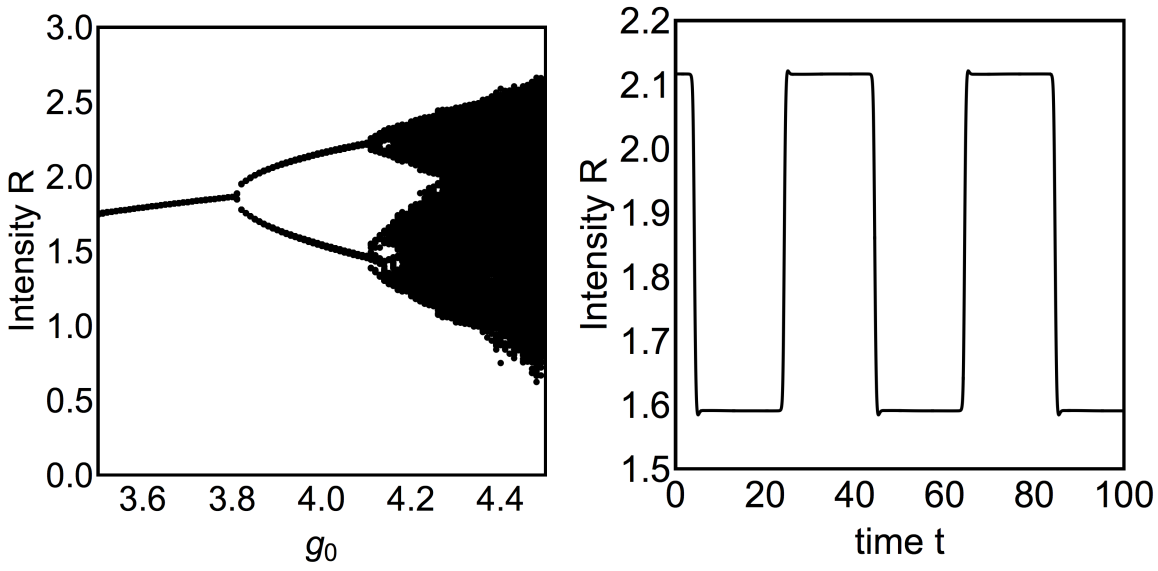

Figure 5: Left: Bifurcation diagram obtained by numerical integration of Eq. (1) with $\kappa = 0.3$, $a = 2$, $T = 20$, and $\gamma = 5$. Right: Square waves calculated numerically for $g_0 = 4.0$. Other parameters are same as for Fig. 5.

5 Mode-locking

Bifurcation diagram in the left panel of Fig. 6 is similar to that shown in Fig. 5, but spans a larger range of the pump parameter values. It follows from this diagram that with the increase of the pump parameter after a chaotic regime associated with the period doubling cascade the phase trajectory of the system jumps to a pulsed solution with time periodic laser intensity. This solution corresponding to a harmonic mode-locked regime with the repetition period close to one half of the cavity round trip time, $T/2$, is illustrated in right panel of Fig. 6. It is seen that the pulses have a fast rise time and a slow decay rate. In the following, we will show that the pulse build-up demonstrates super-exponential growth rate while the decay rate is exponential and is determined by the filter bandwidth γ.

Let us consider a mode-locked solution of Eq. (1) with the period T_0 close to the cavity round trip time T. For this solution satisfying the condition $E(t) = E(t + T_0)$ we can write

$$E(t - T) = E(t - T + T_0) \equiv E(t + \delta) \tag{17}$$

where $\delta = T_0 - T > 0$ is the small difference between the solution period and the delay time. Substituting (17) into (1) we get

$$\gamma^{-1}\frac{dE}{dt} + E = \frac{\sqrt{\kappa}}{2}e^{g_0/[2(1+|E(t+\delta)|^2)]}f(|E(t+\delta)|^2)E(t+\delta). \tag{18}$$

The growth rate of the leading and the decay rate of trailing tail of the mode-locked pulse is determined, respectively, by unstable and stable eigenvalues of the trivial laser off solution $E = 0$ of (18). To find these eigenvalues we linearise (18) at the trivial solution

$$\gamma^{-1}\frac{dE}{dt} + E = \epsilon E(t + \delta), \tag{19}$$

where we have neglected the delayed nonlinear term, but introduced instead of it a linear term proportional to small perturbation parameter ϵ describing an imperfection introduced by a slight asymmetry

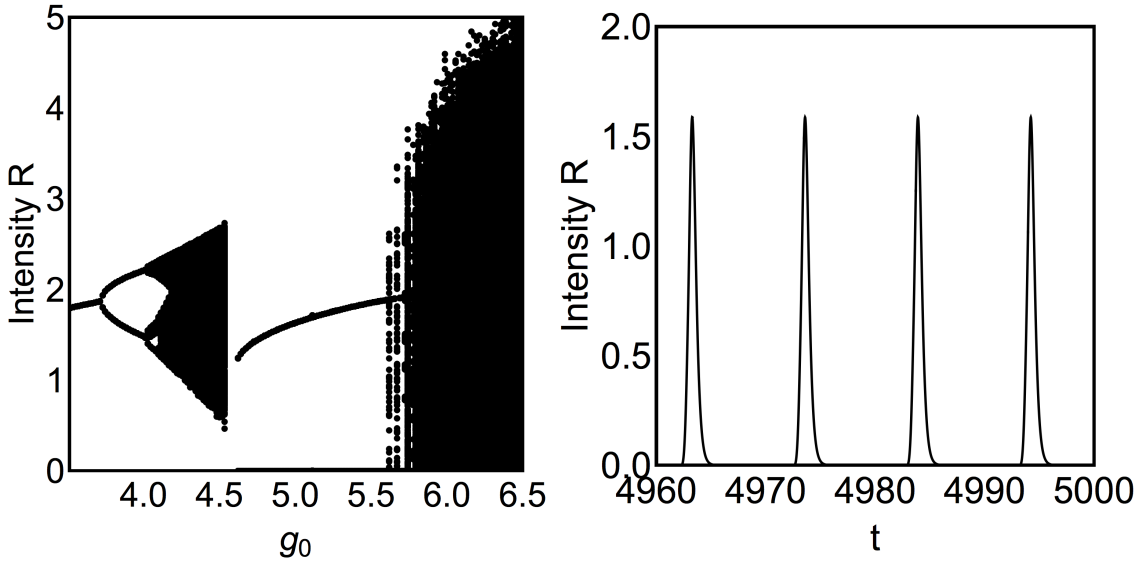

Figure 6: Left: Bifurcation diagram obtained by numerical integration of Eq. (1). Right: harmonic mode-locked regime with two pulses per cavity round trip time calculated for $g_0 = 4.0$. Other parameters are same as for Fig. 5.

of the coupler between the laser cavity the nonlinear mirror loop. The spectrum of Eq. (19) is defined by

$$\lambda_k = -\gamma \left[1 + \frac{W_k(-\epsilon\gamma\delta e^{-\gamma\delta})}{\gamma\delta} \right], \tag{20}$$

where W_k is multivalued Lambert function and the index k numbers different branches of this function. In particular, in the limit $\epsilon \to 0$ the eigenvalue with the index $k = 0$ is the only stable and negative one $\lambda_0 \to -\gamma < 0$. This eigenvalue determines the decay rate of the trailing tail of mode-locked pulse. The remaining eigenvalues with $k \neq 0$ have positive real parts diverging in the limit $\epsilon \to 0$, $\mathrm{Re}\lambda_k \to +\infty$. Among these unstable eigenvalues, the eigenvalue λ_{-1} with $k = -1$ has smallest real and zero imaginary part. All other eigenvalues with $k > 0$ and $k < -1$ have larger real parts and nonzero positive (negative) imaginary parts for negative (positive) k. Hence, generically the eigenvalue λ_{-1} determines the growth rate of the pulse leading edge. The fact that this eigenvalue tends to infinity as $\epsilon \to 0$ suggests that the growth this growth rate is super-exponential.

Finally let us discuss briefly the interaction of asymmetric mode-locked pulses shown in the right panel of Fig. 6. When integrating the model equation (1) numerrically it is possible to seed two or more non-equidistant pulses in the laser cavity as an initial condition. Then the pulses will interact locally via their decaying tails. The asymmetric nature of the pulses suggests that similarly to the case discussed in [24] local interaction of non-equidistant pulses will be very asymmetric as well. This can be is seen in Fig. 7 illustrating an interaction of two asymmetric pulses of Eqs. (1) on the time-round trip number plane. We see that two initially non-equidistant pulses repel each other and become equidistant in the long time limit. Furthermore, when the two pulses are sufficiently close to one another, exponentially decaying trailing tail of the left pulse repels noticeably the right pulse, while the very fast (super-exponentially) decaying leading tail of the right pulse almost does not affect the position of the left pulse. When the pulses become equidistant the interactions from the left and from the right balance each other leading to a stable harmonic mode-locking regime with two pulses per cavity round trip time similar to that shown in the right panel of Fig. 6.

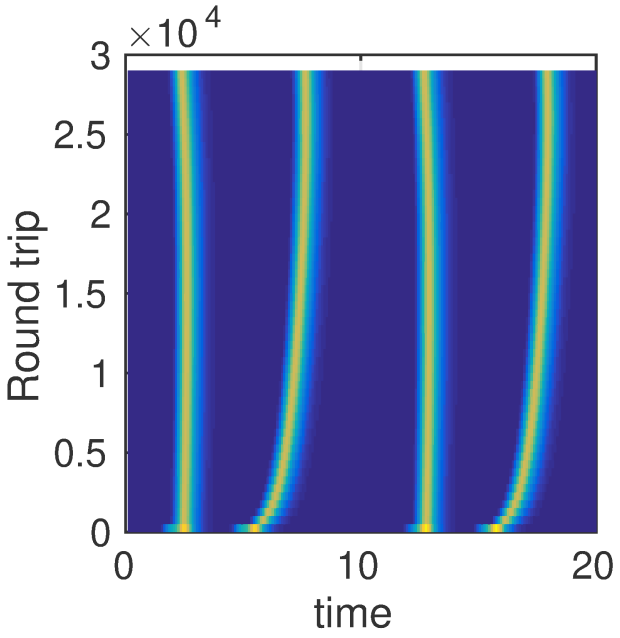

Figure 7: Interaction of two mode-locked pulses leading to a harmonic mode-locked regime with two pulses per cavity round trip $T = 10$. Other parameters are same as for Fig. 5. A common drift of the two interacting pulses is eliminated.

6 Conclusion

We have studied theoretically the dynamical properties of a simple model of unidirectional class-A ring laser including the nonlinear loop mirror. We have performed analytically in the large delay limit linear stability analysis of the CW solitions with constant in time output intensity. We have shown that similarly to the well-known Eckhaus instability only those CW solutions, which belong to the Busse balloon limited by the modulational instability boundary, can be stable. We demonstrated that with the increase of the pump parameter a CW regime looses stability either via a Turing-type instability, or through a bifurcation cascade leading first to a formation of stable square waves, and then to a more complicated square wave patterns with larger and larger periods. We have constructed a 1D map which describes the transition to square waves and their bifurcations. We have shown that the mode-locked pulses, which develop after a chaotic square-wave dynamics are very asymmetric and characterized by super-exponential growth and an exponential decay. The interaction of these pulses is repulsing and very asymmetric as well. It leads to a formation of harmonic mode-locked regimes. Mode-locked pulses always co-exist with the stable laser-off solution. Hence, they can be viewed as temporal cavity solitons having similar properties to spatial and temporal localized structures of light observed in bistable optical systems. The approach based on the DDEs could be used to study the properties of other types of mode-locked lasers including Kerr-lens mode-locked lasers, and model the dynamics of highly nonlinear devices which is of particular interest for applications in the emerging area of reservoir computing.

7 Appendix

The coefficients $c_0(\lambda)$, $c_1(\lambda)$, and c_2 in the characteristic equation (5) are defined by

$$\begin{aligned} c_0(\lambda) &= (\gamma-\lambda)^2+\Omega^2, \\ c_1(\lambda) &= -\frac{a\lambda R(R+1)^2\Omega+\gamma(\gamma-\lambda)[R(2R+4-g_0)+2]+\Omega^2[R(2R+4-g_0)+2]}{(R+1)^2} \\ &- aR\cot\left(\frac{aR}{2}\right)\left(\gamma^2-\gamma\lambda+\Omega^2\right), \\ c_2 &= \frac{\gamma^2\kappa e^{\frac{g_0}{R+1}}}{2(R+1)^2}\{aR(R+1)^2\sin(aR)-[R(R+2-g_0)+1][\cos(aR)-1]\}. \end{aligned}$$

References

[1] A. Aadhi, A. V. Kovalev, M. Kues, P. Roztocki, Ch. Reimer, Y. Zhang, T. Wang, B. E. Little, S. T. Chu, D. J. Moss, Z. Wang, E. Viktorov, and R. Morandotti. Optical square waves from a nonlinear amplifying loop mirror laser (conference presentation), 2018.

[2] R. Arkhipov, A. Pimenov, M. Radziunas, D. Rachinskii, A. G. Vladimirov D., Arsenijević, H. Schmeckebier, and D. Bimberg. Hybrid mode-locking in semiconductor lasers: simulations, analysis and experiments. *IEEE Jornal of Selected Topics in QE*, 99:1100208, 2013.

[3] E. A. Avrutin, J. H. Marsh, and E. L. Portnoi. Monolithic and multi-GigaHerz mode-locked semiconductor lasers: Constructions, experiments, models, and applications. *IEE Proc.-Optoelectron.*, 147:251, 2000.

[4] U. Bandelow, M. Radziunas, J. Sieber, and M. Wolfrum. Impact of gain dispersion on the spatio-temporal dynamics of multisection lasers. *IEEE J. Quantum Electron.*, 37:183–188, 2001.

[5] U. Bandelow, M. Radziunas, A. G. Vladimirov, B. Huettl, and R. Kaiser. 40 GHz modelocked semiconductor lasers: Theory, simulations and experiment. *Optical and Quantum Electronics*, 38(4-6):495–512, 2006.

[6] H. Haus. Modelocking of lasers. *IEEE J. Sel. Top. Quantum Electron.*, 6(6):1173–1185, 2000.

[7] L. C. Jaurigue, B. Krauskopf, and K. Lüdge. Multipulse dynamics of a passively mode-locked semiconductor laser with delayed optical feedback. *Chaos*, 27(11):114301, 2017.

[8] B. Kelleher, M. J. Wishon, A. Locquet, D. Goulding, B. Tykalewicz, G. Huyet, and E. A. Viktorov. Delay induced high order locking effects in semiconductor lasers. *Chaos: An Interdisciplinary Journal of Nonlinear Science*, 27(11):114325, 2017.

[9] M. Kues, Ch. Reimer, B. Wetzel, P. Roztocki, B. E. Little, S. T. Chu, T. Hansson, E. A. Viktorov, D. J. Moss, and R. Morandotti. Passively mode-locked laser with an ultra-narrow spectral width. *Nature Photonics*, 11:159, January 2017.

[10] F. Leo, S. Coen, P. Kockaert, S.-P. Gorza, P. Emplit, and M. Haelterman. Temporal cavity solitons in one-dimensional kerr media as bits in an all-optical buffer. *Nature Photonics*, 4(7):471, 2010.

[11] M. Marconi, J. Javaloyes, S. Balle, and M. Giudici. How lasing localized structures evolve out of passive mode locking. *Phys. Rev. Lett.*, 112:223901, Jun 2014.

[12] C. Otto, K. Lüdge, A. G. Vladimirov, M. Wolfrum, and E. Schöll. Delay-induced dynamics and jitter reduction of passively mode-locked semiconductor lasers subject to optical injection. *New Journal of Physics*, 14:113033, 2012.

[13] A. Pimenov, S. Slepneva, G. Huyet, and A. G. Vladimirov. Dispersive time-delay dynamical systems. *Phys. Rev. Lett.*, 118:193901, May 2017.

[14] A. Pimenov, E. A. Viktorov, S. P. Hegarty, T. Habruseva, G. Huyet, D. Rachinskii, and A. G. Vladimirov. Bistability and hysteresis in an optically injected two-section semiconductor laser. *Phys. Rev. E*, 89:052903, May 2014.

[15] D. Rachinskii, A. G. Vladimirov, U. Bandelow, B. Hüttl, and R. Kaiser. Q-switching instability in a mode-locked semiconductor laser. *J. Opt. Soc. Am. B*, 23(4):663–670, 2006.

[16] N. Rebrova, G. Huyet, D. Rachinskii, and A. G. Vladimirov. Optically injected mode-locked laser. *Physical Review E*, 83:066202, 2011.

[17] S. Slepneva, B. Kelleher, B. O'Shaughnessy, S. P. Hegarty, A. G. Vladimirov, and G. Huyet. Dynamics of fourier domain mode-locked lasers. *Opt. Express*, 21(16):19240–19251, Aug 2013.

[18] S. Slepneva, B. O'Shaughnessy, B. Kelleher, S. P. Hegarty, A. G. Vladimirov, H.-C. Lyu, K. Karnowski, M. Wojtkowski, and G. Huyet. Dynamics of a short cavity swept source oct laser. *Opt. Express*, 22(15):18177–18185, Jul 2014.

[19] B. Tromborg, H. E. Lassen, and H. Olesen. Travelling wave analysis of semiconductor lasers. *IEEE J. Quantum Electron.*, 30:939–956, 1994.

[20] E. A. Viktorov, T. Habruseva, S. P. Hegarty, G. Huyet, and B. Kelleher. Coherence and incoherence in an optical comb. *Phys. Rev. Lett.*, 112:224101, Jun 2014.

[21] E. A. Viktorov, P. Mandel, A. G.Vladimirov, and U. Bandelow. A model for mode-locking in quantum dot lasers. *Appl. Phys. Lett.*, 88:201102 (3 pages), 2006.

[22] E. A. Viktorov, Paul Mandel, and Guillaume Huyet. Long-cavity quantum dot laser. *Opt. Lett.*, 32(10):1268–1270, May 2007.

[23] A. G. Vladimirov, U. Bandelow, G. Fiol, D. Arsenijević, M. Kleinert, D. Bimberg, A. Pimenov, and D. Rachinskii. Dynamical regimes in a monolithic passively mode-locked quantum dot laser. *JOSA B*, 27(10):2102–2109, 2010.

[24] A. G. Vladimirov, S. V. Gurevich, and M. Tlidi. Effect of cherenkov radiation on localized-state interaction. *Physical Review A*, 97(1):013816, 2018.

[25] A. G. Vladimirov and D. Turaev. New model for mode-locking in semiconductor lasers. *Radiophys. & Quant. Electron.*, 47(10-11):857–865, 2004.

[26] A. G. Vladimirov and D. Turaev. Model for passive mode locking in semiconductor lasers. *Physical Review A*, 72(3):033808, 2005.

[27] A. G. Vladimirov, D. Turaev, and G. Kozyreff. Delay differential equations for mode-locked semiconductor lasers. *Opt. Lett.*, 29:1221–1223, 2004.

[28] S. Yanchuk and M. Wolfrum. A multiple time scale approach to the stability of external cavity modes in the Lang-Kobayashi system using the limit of large delay. *SIAM J. Appl. Dyn. Syst.*, 9:519–535, 2010.